ACS APPLIED ELECTRONIC MATERIALS

pubs.acs.org/acsaelm Article

Unusual Sequential Annealing Effect in Achieving High Thermal Stability of Conductive Al-Doped ZnO Nanofilms

Ruolin Yan, Tsunaki Takahashi,* Masaki Kanai, Takuro Hosomi, Guozhu Zhang, Kazuki Nagashima, and Takeshi Yanagida*

Cite This: ACS Appl. Electron. Mater. 2020, 2, 2064−2070 Read Online

ACCESS | Metrics & More | Article Recommendations | Supporting Information

ABSTRACT: Emerging interactive sensor electronics requires metal oxide electrodes that possess long-term atmospheric stability and electrical conductivity to function under harsh conditions (e.g., high temperatures) in air. In this study, we report a rational method to accomplish the long-term thermal stability of conductive Al-doped ZnO (AZO) nanofilms, which have been thermally unstable due to inevitable crystal defects. Our method utilizes a sequential thermal annealing in air and Zn vapor atmosphere. An initial annealing was performed in air, followed by a second annealing in a Zn vapor atmosphere. Air tolerance tests on the resulting AZO nanofilms revealed the stable electrical resistivity ($\sim 10^{-4}$ Ω·cm) in air, even at temperatures up to 500 °C. Conversely, when annealing was performed in the reverse sequence, the electrical resistivity of the AZO nanofilms significantly increased by 5 orders of magnitude during tolerance tests. Photoluminescence data further supported the results of the air tolerance tests. The unusual effect of the annealing−atmosphere sequence is discussed in terms of the presence of dual anion/cation vacancies and the sequential benefits when these vacancies are compensated during annealing. The applicability of these thermally stable AZO electrodes for use in nanochannel sensor devices is demonstrated. Furthermore, we show that the proposed sequential annealing method is applicable for Ga-doped ZnO films, supporting its use as a platform fabrication method. Thus, the proposed fundamental concept for tailoring thermally stable conductive metal oxide electrodes provides a foundation for designing interactive electronic devices that are stable for a long period.

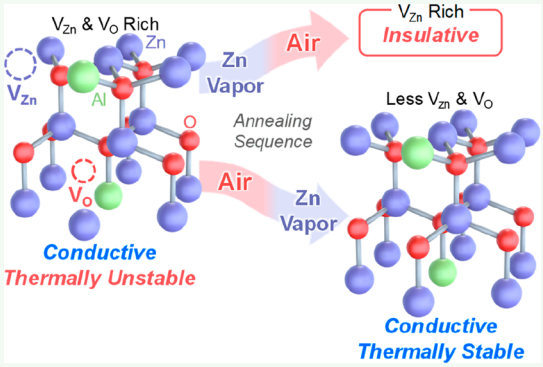

KEYWORDS: *conductive (Al, Ga)-doped ZnO nanofilms, crystal defects, long-term thermally stable electrode, sequential effect of annealing−atmospheres*

INTRODUCTION

Recent advances in interactive electronics seek to collect surrounding physical and chemical information and store them as digital data. Spatially and temporally collected data are utilized to understand various, inherently complex phenomena.[1−4] The interactive electronics inherently requires long-term stability of the electronic material when exposed to air. As conventional electronic materials have been developed in the presence of passivation, designing atmospherically robust and stable electronic materials is a newly emerging area of interest. The inherent stability of conductive metal oxides in air renders them as potential raw materials for robust electrodes in interactive electronics.[5,6]

Conductive metal oxides have been used in various electronic applications including transparent electrodes,[7−11] semiconductor channels,[12−14] and others.[15] Al-doped ZnO (AZO) has been intensively studied due to its high electrical conductivity and abundance of resources. Numerous reports have been published on AZO film fabrications that modulate the deposition parameters during crystal growth, such as oxygen partial pressure, temperature, Al concentration, film thickness, and others.[16−19] A unique finding of these studies is that AZO films grown at lower temperatures are more conductive at the sacrifice of film crystallinity.[18,20] This has been attributed to the thermodynamic stability of aluminum oxides, which hinders Al being as dopants in the AZO crystal structure at relatively high temperatures.[21−23] Thus, as-grown conductive AZO nanofilms contain a substantial amount of various crystal imperfections, which should be closely related to long-term atmospheric stability of the electrical properties of AZO.

Here, we demonstrate the unique sequential thermal annealing effect on the long-term electrical stability of highly conductive AZO nanofilms under atmospheric conditions. We found that only one annealing sequence (initial annealing in air

Received: April 21, 2020
Accepted: June 11, 2020
Published: June 11, 2020

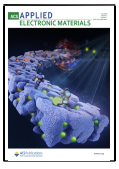

and subsequent annealing in a Zn vapor atmosphere) realizes long-term electrical stability of conductive AZO nanofilms during tolerance test at up to 500 °C in air. This sequence effect of annealing−atmosphere is discussed in terms of the presence of dual anion/cation vacancies and the sequential benefits of compensating vacancies during annealing. In addition, we show the applicability of these thermally stable AZO electrodes in nanochannel chemical sensor devices and the universality of the present concept for Ga-doped ZnO nanofilms.

RESULTS AND DISCUSSION

The electrical resistivity of Al-doped ZnO films (ρ_{AZO}) strongly depends upon various film deposition parameters, including oxygen partial pressures (P_{O_2}), growth temperature (T_s), Al concentration (C_{Al}), thickness (d_t), and deposition rate (v_d). Therefore, we initially focused on the effects of film deposition parameters on ρ_{AZO} to compare AZO nanofilm performance with previously reported investigations from the literature. Figure 1a shows the effects of P_{O_2} and T_s on ρ_{AZO}. For these

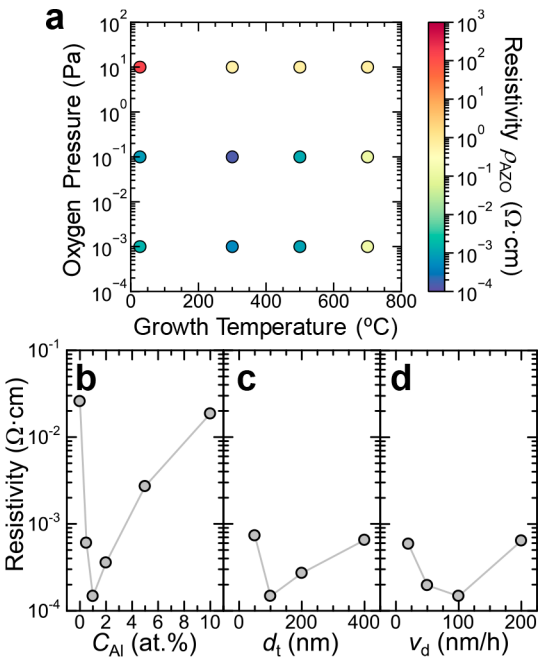

Figure 1. Effects of PLD parameters on resistivity of AZO nanofilms ρ_{AZO}. (a) Oxygen pressure and growth temperature, (b) Al atomic concentration C_{Al} in the AZO target, (c) film thickness d_t, and (d) deposition rate v_d. The oxygen pressure, growth temperature, C_{Al}, d_t, and v_d were set to 10^{-1} Pa, 300 °C, 1 at. %, 100 nm, and 100 nm/h, respectively, except for specifically mentioned cases.

experiments, C_{Al}, d_t, and v_d were held constant at 1%, 100 nm, and 100 nm/h, respectively. ρ_{AZO} tends to be lower at lower P_{O_2} and T_s values. A minimum ρ_{AZO} (~10^{-4} Ω·cm) appears at approximately P_{O_2} = 10^{-1} Pa and T_s = 300 °C, which is consistent with previous studies.[8,17,21,24] The reduction of ρ_{AZO} at low P_{O_2} and T_s has been interpreted in terms of the stability of oxygen vacancies and the prevention of aluminum oxide segregation during AZO film deposition.[18,21] Figures 1b−d show the effects of C_{Al}, d_t, and v_d on the ρ_{AZO}. For these experiments, P_{O_2} and T_s were held constant at 10^{-1} Pa and 300 °C, respectively. ρ_{AZO} initially decreased but then increased with increasing C_{Al}. The optimum C_{Al} is interpreted as a competing effect of aluminum oxide formation and Al donor activation within the ZnO structure during film deposition.[17,25] The remaining deposition parameters (d_t and v_d) do not significantly affect ρ_{AZO} when compared with the effects of P_{O_2}, T_s, and C_{Al} within the range of this study. Through these experiments, deposition parameters were optimized to achieve AZO films with high electrical conductivity (~10^{-4} Ω·cm) which are comparable to ρ_{AZO} reported in the literature.[13,16,26] The optimized deposition condition was utilized for further investigation of atmospheric thermal stability of AZO nanofilms.

The long-term atmospheric stability of ρ_{AZO} was investigated by using the optimized electrically conductive AZO films. Figure 2a shows the temporal change of ρ_{AZO} when as-grown AZO films were exposed to air at 400 °C. ρ_{AZO} significantly increased by 9 orders of magnitude from 10^{-4} to 10^{5} Ω·cm within 100 h of exposure time. As shown in Figure 2b, such electrical degradation of as-grown AZO films occurred at temperatures above 200 °C, and degradation of electrical conductivity accelerates with increasing temperature. Thus, the electrically conductive, as-grown AZO films are not thermally stable electrodes when exposed long term to atmospheric conditions.

To enhance the thermal stability in ambient air, we applied thermal annealing processes to AZO nanofilms before the tolerance tests; this was aimed to compensate for the crystal imperfections introduced to the nanofilms during the formation process.[27,28] Figure 2c illustrates the annealing processes employed to enhance film stability. Because previous studies have reported that Zn vapor (Zn-rich) annealing is effective to enhance thermal stability of ρ_{AZO} through compensation of Zn vacancies in AZO films,[21,29] we applied Zn vapor annealing to our as-grown AZO nanofilms. In addition to the one-step Zn vapor annealing, two-step sequential annealings, which are called sequence I (annealing in Zn vapor followed by air) and II (annealing in air and then Zn vapor) in Figure 2c, were also performed to investigate the effects of oxygen vacancy compensation. Figure 2d shows thermal tolerance tests of ρ_{AZO} of these annealed AZO nanofilms. Interestingly, only sequence II annealing resulted in a low ρ_{AZO} (10^{-4}−10^{-3} Ω·cm) during tolerance tests even at test temperatures of up to 500 °C, whereas the one-step Zn vapor annealing could not enhance the thermal stability. The superior thermal stability of ρ_{AZO} via sequence II is clear evidence of the impacts of the process before the last annealing, which is the sequential annealing effect, because the last step of sequence II is the same as the one-step Zn vapor annealing. Similar to one-step Zn vapor annealing, sequence I annealing also could not enhance the thermal stability of ρ_{AZO} and even degrades electrical conductivity after thermal load of less than 300 °C. The stable ρ_{AZO} of AZO nanofilms via sequence II compared with that via sequence I was also observed in temporal thermal tolerance tests at 400 °C in air (Supporting Information Figure S1). Although the difference between the two annealing sequences I and II is solely the order of annealing atmospheres, its effect on the thermal stability of ρ_{AZO} is remarkable.

The physical properties of annealed AZO films were measured to understand the mechanism that causes the effect of sequential annealing atmospheres on ρ_{AZO}. Figures 3a,b show the comparison between the X-ray diffraction (XRD) and

https://dx.doi.org/10.1021/acsaelm.0c00321
ACS Appl. Electron. Mater. 2020, 2, 2064−2070

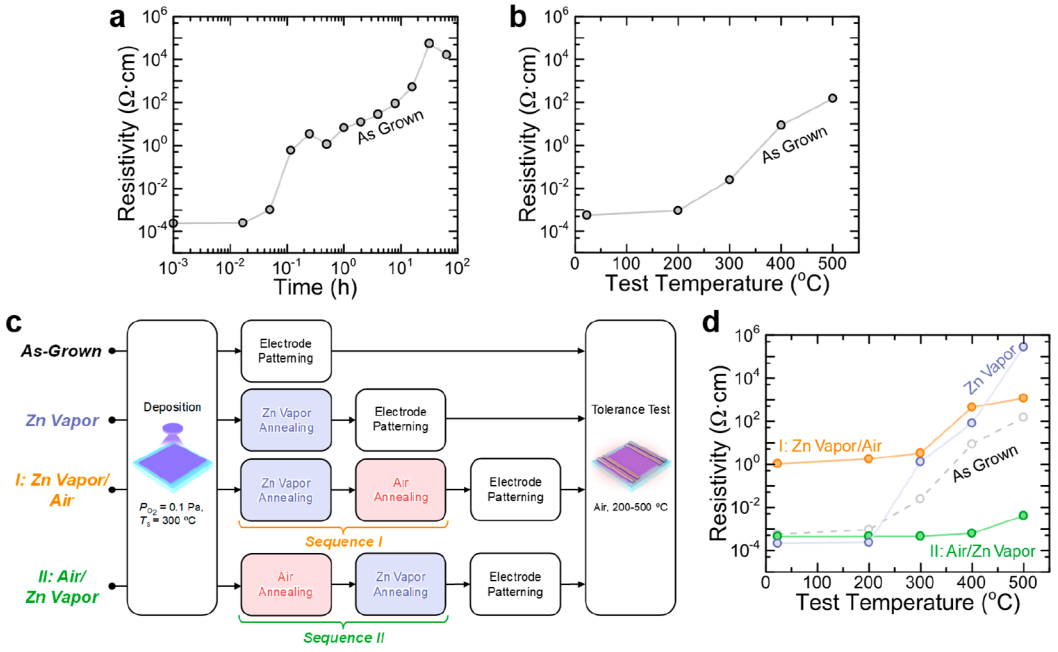

Figure 2. Thermal tolerance tests of resistivity of as-grown AZO nanofilms (a) at 400 °C for varied thermal stress time in air and (b) at varied test temperature for 1 h in air. (c) Flowchart of annealing procedures including sequential annealings of sequence I and II. (d) Thermal tolerance tests of resistivity of annealed AZO nanofilms at varied test temperatures for 1 h in air. Test results of the as-grown AZO nanofilm are also shown for comparison. All resistivity measurements were performed at room temperature.

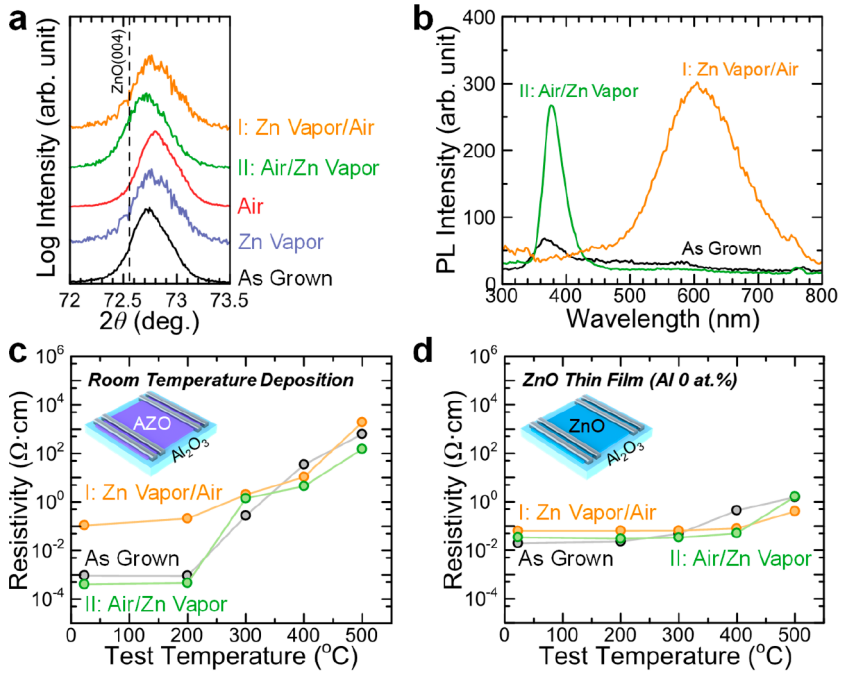

Figure 3. (a) XRD patterns of AZO nanofilms for sequence I (Zn vapor/air) annealed, sequence II (air/Zn vapor) annealed, air annealed, Zn vapor annealed, and as-grown samples. (b) PL spectrum of AZO nanofilms for sequence I annealed, sequence II annealed, and as-grown samples. Effects of thermal tolerance test temperature on resistivities of (c) AZO nanofilms grown at room temperature and (d) ZnO nanofilms (Al 0 at. %) samples. All thermal tolerance tests were performed in ambient air for 1 h.

photoluminescence (PL) of as-grown, sequence I, and sequence II AZO nanofilms. Although annealing alters the AZO lattice constant toward the bulk value in the XRD data, their full width at half-maximum (FWHM) variation is minimal (0.36−0.43), indicating that the annealing effect on the crystal structure is not significant like a structural change from amorphous to crystal. The morphology of AZO nanofilms also did not change significantly after the sequential annealings (Figure S2). However, a substantial difference can be seen in the PL data between sequence I and sequence II nanofilms. AZO nanofilms annealed by sequence I exhibited a broad luminescence around 600 nm due to crystal imperfections. Although identification of the types of crystal imperfection within the AZO nanofilm is difficult due to the

https://dx.doi.org/10.1021/acsaelm.0c00321
ACS Appl. Electron. Mater. 2020, 2, 2064−2070

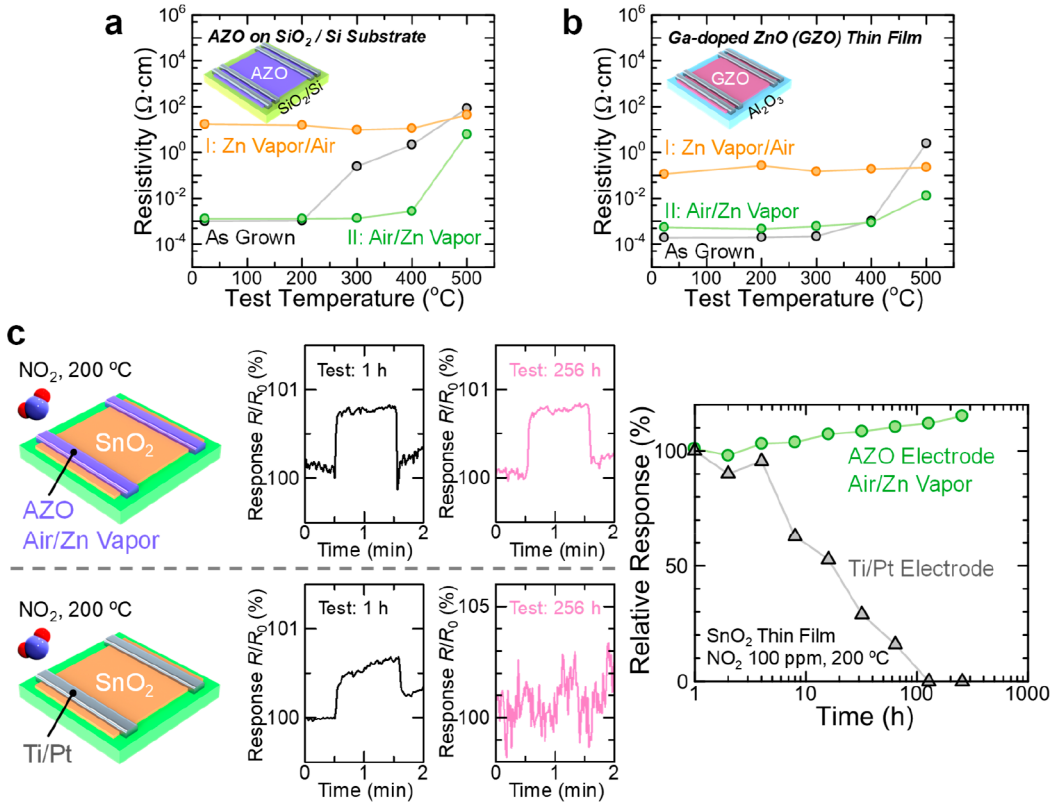

Figure 4. Effects of thermal tolerance test temperature on resistivities of (a) AZO nanofilms grown on a SiO_2/Si substrate and (b) Ga-doped ZnO (GZO) nanofilms. All thermal tolerance tests were performed in ambient air for 1 h. (c) 100 ppm of NO_2 sensing properties of SnO_2 nanochannel sensor devices with the electrodes of sequence II (air/Zn vapor) annealed AZO or Ti/Pt. Time series sensing characteristics after 1 and 256 h thermal test under sensor operation conditions (200 °C, ambient air) are shown. The relationship between relative sensor response and test duration (200 °C, ambient air) is also shown.

broad peak, the previous studies have reported that this luminescent range contains emissions originated in oxygen/Zn vacancies and interstitials, antisite oxygen, and combinations of them.[30−32] On the other hand, AZO nanofilms annealed by sequence II showed only an ultraviolet emission peak at ∼380 nm, which originates from excitonic-related transitions, without the broad luminescence around 600 nm related to crystal imperfections. Thus, AZO nanofilms annealed by sequence II contain fewer crystal imperfections when compared with other AZO nanofilms. Notably, the low-defect structure of the sequence II sample was maintained after the thermal tolerance tests, whereas crystal imperfections of the as-grown sample significantly increased during the thermal tolerance tests (Figure S3). These results imply that the observed effect of annealing atmosphere sequence on the stability of ρ_{AZO} is closely related to the crystal imperfections within the AZO nanofilms. This correlation is further consistent with tolerance test results when varying the film deposition parameters. Figure 3c shows the thermal tolerance of ρ_{AZO} for AZO nanofilms deposited at room temperature, which lowers the film crystallinity compared with nanofilms deposited at 300 °C (Figure S4). There is almost no effect of the annealing−atmosphere sequence on the stability of ρ_{AZO} under atmospheric conditions. Furthermore, the effect of annealing sequence is not observed in nondoped ZnO nanofilms (Figure 3d), suggesting that this sequential effect requires Al dopants within the films. Thus, these results suggest that the observed sequential annealing effect on the stability of ρ_{AZO} is closely related to the degree of crystal imperfections in AZO crystalline nanofilms when Al dopants are present.

The above results highlight that the annealing sequence significantly affects the thermal stability of ρ_{AZO}, and at the same time, one-step Zn vapor annealing results in the degraded thermal stability compared with Zn vapor annealing after air annealing (sequence II), as shown in Figure 2d. Thus, it is obvious that the thermal stability cannot be determined only by the last annealing atmosphere, and the initial state before the last annealing critically determines the final thermal stability. Because XRD data of AZO with sequence II annealing show a similar FWHM and slightly different *d*-value from others (Figure 3a), the most plausible origin of the annealing-sequence-dependent thermal stability must be slight difference of chemical composition among these annealed samples. One simple model which can explain the sequential annealing effects is that the defect compensation via annealing process is limited by the balance of ion content in the initial state before annealing process. This model is supported by the obtained PL spectrum which indicates the lower crystal imperfections in the sequence II sample (Figure 3b). The high electrical conductivity of the optimized as-grown AZO (n-type) utilized for the stability tests (Figure 1) suggests the ion contents of excess cation (Zn ion) and insufficient anion (oxygen ion). Therefore, the cation defect compensation via Zn vapor annealing must be limited because the initial state is already cation excess. On the other hand, air annealing of the as-grown AZO can effectively compensate for anion defects due to the insufficient anion content at the initial state and may

https://dx.doi.org/10.1021/acsaelm.0c00321
ACS Appl. Electron. Mater. 2020, 2, 2064−2070

realize balanced cation/anion content. After realizing the balanced ion content via air annealing, Zn vapor annealing can supply sufficient Zn ion into AZO because of their weak limitation of defect compensation in each annealing step (see the Supporting Information for a detailed discussion). Therefore, this procedure (sequence II, annealing in air and then in Zn vapor) yields smaller defect contents in the AZO film than that of the one-step Zn vapor annealed samples. In sequence I (annealing in Zn vapor then in air), anion defect compensation with the last air annealing must be enough, but the cation defect will remain at the final state due to the limited Zn incorporation at the first Zn vapor annealing. Thus, the smaller defect content with sequence II annealing than that with sequence I or one-step Zn vapor annealing can be the reason the AZO nanofilm annealed by sequence II only exhibits the superior thermal stability of ρ_{AZO} than others. The ρ_{AZO} of sequence II samples slightly increases during the thermal tolerance tests (Figure 2d), possibly due to nanoscale aluminum oxide formation within AZO and/or Zn vaporization from the surface at high temperatures.[17,25,33] We did not observe any sequential annealing effect in the nondoped ZnO nanofilms (Figure 3d), implying that an excess of n-type carriers generated by Al dopants were responsible for the sequential annealing effect. Because the amount of n-type carriers affects the effectiveness of compensation of anion/cation defects through charge neutrality, the observed results are consistent with the proposed model (see the Supporting Information for a detailed discussion). The room-temperature-grown AZO nanofilms (Figure 3c), which are amorphous-like in structure (Figure S4), also did not show the sequential effect, supporting the model based on a correlation of crystal imperfections in ZnO with the sequential annealing effects. Furthermore, both the observed sequential annealing effect and the previous study of Zn vapor annealing[21,29] can be consistently explained as follows. Figure 2d shows that properties of AZO after Zn vapor annealing are strongly affected by its oxygen content before the annealing, and Zn vapor annealing of the AZO with sufficiently high oxygen content can achieve high thermal stability. Because the starting material (as-grown AZO nanofilm) in this paper has low resistivity less than 10^{-3} Ω·cm (Figure 1a), corresponding to a relatively high amount of oxygen defect, the air annealing before Zn vapor annealing is necessary to decrease the oxygen defect and enhance thermal stability. On the other hand, the starting material in the previous reports[21,29] had the high resistivity (>10^{3} Ω·cm) which indicates less oxygen defect. Therefore, one-step Zn vapor annealing could enhance the thermal stability of ρ_{AZO} in these studies.

The sequential annealing effect on the atmospheric stability of ρ_{AZO} is demonstrated for AZO nanofilms grown on a single-crystalline sapphire substrate. To examine the applicability of this sequential methodology, we applied the present sequential annealing process to AZO nanofilms grown on a thermal-SiO_2 (amorphous)/Si substrate which is utilized in a wide variety of electronic applications. Figure 4a shows the thermal tolerance test of ρ_{AZO} for AZO nanofilms grown on SiO_2/Si substrates. AZO nanofilms annealed by sequence II exhibited thermal stability of electrical conductivity at atmospheric conditions, similar to results of AZO nanofilms grown on sapphire substrates (Figure 2). The effects of sequence II annealing were further observed in Ga-doped ZnO (GZO) nanofilms (Figure 4b). The results of the tolerance tests on AZO nanofilms grown on SiO_2/Si substrates and GZO nanofilms strongly support the universality of the sequential effect of annealing atmospheres. We also confirmed that the ρ_{AZO} of AZO nanofilms annealed by sequence II shows better atmospheric thermal stability than that of previous studies with various methods[20,21,29,34] (Figure S5). Figure 4c shows the applicability of the present atmospherically and thermally stable AZO electrodes for nanochannel chemical sensor devices. In Figure 4c, long-term stability of sensor response to 100 ppm of NO_2 is evaluated at 200 °C by using SnO_2 nanochannel sensors with sequence-II-annealed AZO and conventional metal (Ti/Pt) electrodes. Details of the sensor device fabrication and sensing measurements are described in the Methods section. The sensor responses of SnO_2 nanochannel sensors with metal electrodes and sequence-I-annealed AZO electrodes (see Figure S6) rapidly degrade due to insulation of electrodes (Ti or AZO) in the sensing condition at high temperature in atmospheric air. On the other hand, the nanochannel sensors with sequence-II-annealed AZO electrodes impart the long-term stability of its NO_2-sensing properties compared with the sensors using other two types of electrodes. The response of nanochannel sensor with sequence-II-annealed AZO electrodes increases gradually during the stability test. The improvement of the sensor response is possibly due to a removal of residual organic compounds and/or reduction of adsorbed oxygen on the SnO_2 surface during the long-term heating and sensor measurements in a N_2 atmosphere.[35,36] Note that the improvement was not observed in the sensors with the other two types of electrodes because of the rapid insulation of the electrodes discussed above. Thus, the series of results indicates a feasibility of applications using the proposed sequential annealing method.

CONCLUSION

We demonstrate a rational method to accomplish conductive Al-doped ZnO (AZO) nanofilms with long-term stability in air. Our method is based upon a sequential compensation effect of anion/cation vacancies within AZO nanofilms. When annealing is first performed in air and then in a Zn vapor atmosphere (sequence II), the electrical resistivity of AZO nanofilms is stable (~10^{-4} Ω·cm), even under temperatures of up to 500 °C in air during thermal tolerance tests. Conversely, when the annealing process is performed in the reverse sequence (sequence I), the electrical resistivity of AZO nanofilms significantly increases by 5 orders of magnitude during thermal tolerance tests. Photoluminescence data reveal a greater amount of crystal imperfections in AZO nanofilms that underwent sequence I treatment compared to sequence II. This sequential effect of annealing atmospheres is discussed in terms of the presence of dual anion/cation vacancies and the sequential benefits when compensating those vacancies during annealing. Furthermore, we show that the proposed sequential annealing concept is applicable for Ga-doped ZnO films, supporting its use as a platform annealing method. The applicability of these thermally stable AZO electrodes for nanochannel sensors is demonstrated. Because the proposed fundamental concept can be applied to nanofilms made of various materials, it provides a foundation for designing interactive electronic devices that have long-term stability.

METHODS

ZnO Nanofilm Fabrication. Doped and undoped ZnO nanofilms were deposited on Al_2O_3 (110) or 100 nm SiO_2/n-type Si substrates by the pulsed-laser deposition (PLD) method.[5,26] For the Al- or Ga-

https://dx.doi.org/10.1021/acsaelm.0c00321
ACS Appl. Electron. Mater. 2020, 2, 2064−2070

doped ZnO nanofilms (AZO or GZO), sintered tablets (controlled at. % of Al_2O_3 or 1 at. % of Ga_2O_3 in ZnO, 99.99% purity, Kojundo Chemical Laboratory) were utilized as targets for ablation by an ArF excimer laser (λ = 193 nm, Coherent, COMPex Pro). For the undoped ZnO nanofilms, a tablet of the ZnO source (99.99% purity, Kojundo Chemical Laboratory) was utilized as the target for ablation. The chamber for deposition was initially evacuated below 5×10^{-6} Pa, following which an oxygen gas (purity: 99.9999%) was introduced with controlled oxygen pressure in the range 10^{-3}−10 Pa. The oxygen pressure, growth temperature, Al atomic concentration in the AZO target, film thickness, and deposition rate were set to 10^{-1} Pa, 300 °C, 1 at. %, 100 nm, and 100 nm/h, respectively, except for specifically mentioned cases. A part of the deposited nanofilms was then sequentially annealed in the two types of conditions: (i) ambient air, 500 °C, and 1 h or (ii) Zn vapor, 600 °C, and 1 h. For Zn vapor annealing, samples were put into a small crucible with a Zn tablet (99.99% pure, Kojundo Chemical Laboratory) and maintained in 0.1 Pa at 600 °C for 1 h.[21,29] The distance between samples and Zn tablet is 3 cm, and the AZO-deposited side of sample substrates was downward to prevent direct Zn deposition on the AZO surface. Then the crucible was sealed in a quartz tube and evacuated to 0.1 Pa, followed by temperature increase to 600 °C at a heating rate of 20 °C/min. In sequence I, samples were annealed first in Zn vapor and then in air (Zn vapor/air). In sequence II, samples were annealed first in air and then in Zn vapor (air/Zn vapor).

ZnO Nanofilm Characterizations. Electrical resistivities of the fabricated ZnO nanofilms were measured by the four-probe technique using a semiconductor parameter analyzer (Keithley, 4200SCS) with a probe station at room temperature. Electrodes for the ZnO nanofilm devices were fabricated by depositing 100 nm of Pt by a radio-frequency (RF) sputtering using a stencil mask. The PL spectra of ZnO nanofilms on Al_2O_3 (110) substrates were measured by a spectrofluorometer (JASCO, FP-8500) with a Xe lamp source and a fixed excitation wavelength of 256 nm. Structural characterizations of ZnO nanofilms were performed using XRD (PHILIPS, X'Pert MRD 45 kV, 40 mA, Cu Kα source, 1.54 Å). Thermal tolerance tests of the fabricated ZnO nanofilm devices were performed in ambient air at temperatures ranging from room temperature to 500 °C for a controlled period. Electrical resistivities were measured in ambient air at room temperature after each thermal stress.

Sensor Devices. 200 nm of SnO_2 was deposited and patterned on a 100 nm SiO_2/n-type Si substrate by using a RF sputtering and lift-off process of electron beam (EB) lithography. 100 nm AZO or 20 nm Ti/100 nm Pt was then deposited and patterned by using a PLD or RF sputtering and lift-off processes of EB lithography, respectively, as two-terminal electrodes. The thin Ti layer in the Ti/Pt electrodes was deposited as an adhesion layer to avoid peeling off of electrodes from SiO_2 on a Si substrate.[37,38] These electrode depositions were performed at room temperature. AZO contact devices were annealed after the electrode fabrication using sequence I or II. SnO_2 nanofilms for Ti/Pt electrode devices were also annealed in sequence II before electrode deposition to compensate for the difference in SnO_2 resistivity between AZO and Ti/Pt electrode devices. In the sensor characterizations, N_2-balanced 100 ppm of NO_2 gas was introduced into the probe station chamber. The sensor resistance under pure N_2 flow was defined as R_0. The sensor response was extracted as $(R/R_0) \times 100\%$, where R is the sensor resistance. The thermal loads during intervals between the sensor measurements were applied in ambient air at 200 °C.

■ ASSOCIATED CONTENT

Supporting Information

The Supporting Information is available free of charge at https://pubs.acs.org/doi/10.1021/acsaelm.0c00321.

Temporal thermal tolerance tests of sequentially annealed AZO; morphology of AZO nanofilms; PL spectra of AZO nanofilms after thermal tolerance tests; sequential annealing effect; effects of growth temperature on the crystallinity of AZO; benchmark of conductivity of AZO; sensor properties of SnO_2 nanochannel sensors with Zn vapor/air annealed AZO electrodes (PDF)

■ AUTHOR INFORMATION

Corresponding Authors

Tsunaki Takahashi − *Department of Applied Chemistry, Graduate School of Engineering, The University of Tokyo, Tokyo 113-8656, Japan; JST, PRESTO, Kawaguchi, Saitama 332-0012, Japan;* orcid.org/0000-0002-2840-8038; Email: takahashi-t@g.ecc.u-tokyo.ac.jp

Takeshi Yanagida − *Institute for Materials Chemistry and Engineering, Kyushu University, Kasuga, Fukuoka 816-8580, Japan; Department of Applied Chemistry, Graduate School of Engineering, The University of Tokyo, Tokyo 113-8656, Japan;* orcid.org/0000-0003-4837-5701; Email: yanagida@g.ecc.u-tokyo.ac.jp

Authors

Ruolin Yan − *Institute for Materials Chemistry and Engineering, Kyushu University, Kasuga, Fukuoka 816-8580, Japan*

Masaki Kanai − *Institute for Materials Chemistry and Engineering, Kyushu University, Kasuga, Fukuoka 816-8580, Japan*

Takuro Hosomi − *Department of Applied Chemistry, Graduate School of Engineering, The University of Tokyo, Tokyo 113-8656, Japan; JST, PRESTO, Kawaguchi, Saitama 332-0012, Japan;* orcid.org/0000-0002-5649-6696

Guozhu Zhang − *Institute for Materials Chemistry and Engineering, Kyushu University, Kasuga, Fukuoka 816-8580, Japan*

Kazuki Nagashima − *Institute for Materials Chemistry and Engineering, Kyushu University, Kasuga, Fukuoka 816-8580, Japan; JST, PRESTO, Kawaguchi, Saitama 332-0012, Japan;* orcid.org/0000-0003-0180-816X

Complete contact information is available at: https://pubs.acs.org/10.1021/acsaelm.0c00321

Notes

The authors declare no competing financial interest.

■ ACKNOWLEDGMENTS

This work was supported by KAKENHI (Grants JP17H04927, JP18H01831, JP18H05243, and JP18KK0112). R.Y. was supported by the program of China Scholarships Council (No. 201706090261). T.T. was supported by JST PRESTO, Japan (Grant JPMJPR19M6). T.T., T.H., K.N., and T.Y. were supported by JST CREST, Japan (Grant JPMJCR19I2). T.Y. and K.N. were supported by CAS-JSPS Joint Research Projects (Grant JPJSBP120187207). This work was performed under the Cooperative Research Program of "Network Joint Research Center for Materials and Devices" and the MEXT Project of "Integrated Research Consortium on Chemical Sciences".

■ REFERENCES

(1) Chen, L.; Liu, R.; Liu, Z.-P.; Li, M.; Aihara, K. Detecting early-warning signals for sudden deterioration of complex diseases by dynamical network biomarkers. *Sci. Rep.* **2012**, *2*, 1−8.

(2) Tanaka, T.; Hoshino, S.; Takahashi, T.; Uchida, K. Nanoscale Pt thin film sensor for accurate detection of ppm level hydrogen in air at high humidity. *Sens. Actuators, B* **2018**, *258*, 913−919.

(3) Peng, R. D.; Bell, M. L. Spatial misalignment in time series studies of air pollution and health data. *Biostatistics* **2010**, *11*, 720−740.
(4) Peng, G.; Tisch, U.; Adams, O.; Hakim, M.; Shehada, N.; Broza, Y. Y.; Billan, S.; Abdah-Bortnyak, R.; Kuten, A.; Haick, H. Diagnosing lung cancer in exhaled breath using gold nanoparticles. *Nat. Nanotechnol.* **2009**, *4*, 669−673.
(5) Kodu, M.; Arroval, T.; Avarmaa, T.; Jaaniso, R.; Kink, I.; Leinberg, S.; Savi, K.; Timusk, M. Effect of oxygen on active Al concentration in ZnO:Al thin films made by PLD. *Appl. Surf. Sci.* **2014**, *320*, 756−763.
(6) Zeng, H.; Takahashi, T.; Kanai, M.; Zhang, G.; He, Y.; Nagashima, K.; Yanagida, T. Long-Term Stability of Oxide Nanowire Sensors via Heavily Doped Oxide Contact. *ACS Sens.* **2017**, *2*, 1854−1859.
(7) Lin, Y.; Chen, T.; Wang, L.; Lien, S. Comparison of AZO, GZO, and AGZO thin films TCOs applied for a-Si solar cells. *J. Electrochem. Soc.* **2012**, *159* (6), H599−H604.
(8) Kim, H.; Gilmore, C. M.; Horwitz, J. S.; Piqué, A.; Murata, H.; Kushto, G. P.; Schlaf, R.; Kafafi, Z. H.; Chrisey, D. B. Transparent conducting aluminum-doped zinc oxide thin films for organic light-emitting devices. *Appl. Phys. Lett.* **2000**, *76* (3), 259−261.
(9) Nanto, H.; Minami, T.; Shooji, S.; Takata, S. Electrical and optical properties of zinc oxide thin films prepared by rf magnetron sputtering for transparent electrode applications. *J. Appl. Phys.* **1984**, *55* (4), 1029−1034.
(10) Nomoto, J.-i.; Hirano, T.; Miyata, T.; Minami, T. Preparation of Al-doped ZnO transparent electrodes suitable for thin-film solar cell applications by various types of magnetron sputtering depositions. *Thin Solid Films* **2011**, *520* (5), 1400−1406.
(11) Meyer, J.; Görrn, P.; Hamwi, S.; Johannes, H. H.; Riedl, T.; Kowalsky, W. Indium-free transparent organic light emitting diodes with Al doped ZnO electrodes grown by atomic layer and pulsed laser deposition. *Appl. Phys. Lett.* **2008**, *93* (7), 073308.
(12) Fine, G. F.; Cavanagh, L. M.; Afonja, A.; Binions, R. Metal oxide semi-conductor gas sensors in environmental monitoring. *Sensors* **2010**, *10* (6), 5469−502.
(13) Kim, H.; Pique, A.; Horwitz, J. S.; Murata, H.; Kafafi, Z. H.; Gilmore, C. M.; Chrisey, D. B. Effect of aluminum doping on zinc oxide thin films grown by pulsed laser deposition for organic light-emitting devices. *Thin Solid Films* **2000**, *377*−*378*, 798−802.
(14) Chen, H.; Liu, H.; Zhang, Z.; Hu, K.; Fang, X. Nanostructured photodetectors: From ultraviolet to terahertz. *Adv. Mater.* **2016**, *28* (3), 403−33.
(15) Lin, D. D.; Wu, H.; Pan, W. Photoswitches and memories assembled by electrospinning aluminum-doped zinc oxide single nanowires. *Adv. Mater.* **2007**, *19* (22), 3968−3972.
(16) Agura, H.; Suzuki, A.; Matsushita, T.; Aoki, T.; Okuda, M. Low resistivity transparent conducting Al-doped ZnO films prepared by pulsed laser deposition. *Thin Solid Films* **2003**, *445* (2), 263−267.
(17) Liu, Y.; Lian, J. Optical and electrical properties of aluminum-doped ZnO thin films grown by pulsed laser deposition. *Appl. Surf. Sci.* **2007**, *253* (7), 3727−3730.
(18) Dong, B.-Z.; Hu, H.; Fang, G.-J.; Zhao, X.-Z.; Zheng, D.-Y.; Sun, Y.-P. Comprehensive investigation of structural, electrical, and optical properties for ZnO:Al films deposited at different substrate temperature and oxygen ambient. *J. Appl. Phys.* **2008**, *103* (7), 073711.
(19) Chu, J.; Ma, J.; Liang, Y.; Yao, N.; Zhu, X.; Jiang, J.; Chu, J.; Wang, C. Effects of post annealing on structural, electrical and optical properties of ZnO:Al thin films prepared by RF magnetron sputtering. *Proc. SPIE* **2013**, *9068*, 90680F.
(20) Lee, S.; Park, Y.; Kim, D.; Baek, D.; Yi, J.; Hong, B.; Choi, W.; Lee, J. Thermal stability of hydrogen-doped AZO thin films for photovoltaic applications. *Mater. Res. Bull.* **2014**, *58*, 126−131.
(21) Zhan, Z.; Zhang, J.; Zheng, Q.; Pan, D.; Huang, J.; Huang, F.; Lin, Z. Strategy for preparing Al-doped ZnO thin film with high mobility and high stability. *Cryst. Growth Des.* **2011**, *11* (1), 21−25.
(22) Bayraktaroglu, B.; Leedy, K.; Bedford, R. High temperature stability of postgrowth annealed transparent and conductive ZnO:Al films. *Appl. Phys. Lett.* **2008**, *93*, 022104.
(23) T-Thienprasert, J.; Rujirawat, S.; Klysubun, W.; Duenow, J. N.; Coutts, T. J.; Zhang, S. B.; Look, D. C.; Limpijumnong, S. Compensation in Al-doped ZnO by Al-related acceptor complexes: synchrotron x-ray absorption spectroscopy and theory. *Phys. Rev. Lett.* **2013**, *110* (5), 055502.
(24) Guillén, C.; Herrero, J. Optical, electrical and structural characteristics of Al:ZnO thin films with various thicknesses deposited by DC sputtering at room temperature and annealed in air or vacuum. *Vacuum* **2010**, *84* (7), 924−929.
(25) Hu, J.; Gordon, R. G. Textured aluminum-doped zinc oxide thin films from atmospheric pressure chemical-vapor deposition. *J. Appl. Phys.* **1992**, *71* (2), 880−890.
(26) Singh, A. V.; Mehra, R. M.; Buthrath, N.; Wakahara, A.; Yoshida, A. Highly conductive and transparent aluminum-doped zinc oxide thin films prepared by pulsed laser deposition in oxygen ambient. *J. Appl. Phys.* **2001**, *90* (11), 5661−5665.
(27) Oba, F.; Togo, A.; Tanaka, I.; Paier, J.; Kresse, G. Defect energetics in ZnO: A hybrid Hartree-Fock density functional study. *Phys. Rev. B: Condens. Matter Mater. Phys.* **2008**, *77* (24), 245202.
(28) Lany, S.; Zunger, A. Dopability, intrinsic conductivity, and nonstoichiometry of transparent conducting oxides. *Phys. Rev. Lett.* **2007**, *98* (4), 045501.
(29) Hu, Q. C.; Ding, K.; Zhang, J. Y.; Yan, F. P.; Pan, D. M.; Huang, F.; Chiou, J. W. On the variations of optical property and electronic structure in heavily Al-doped ZnO films during double-step growth process. *Appl. Phys. Lett.* **2014**, *104* (2), 021913.
(30) Xing, G. Z.; Lu, Y. H.; Tian, Y. F.; Yi, J. B.; Lim, C. C.; Li, Y. F.; Li, G. P.; Wang, D. D.; Yao, B.; Ding, J.; Feng, Y. P.; Wu, T. Defect-induced magnetism in undoped wide band gap oxides: Zinc vacancies in ZnO as an example. *AIP Adv.* **2011**, *1* (2), 022152.
(31) Lin, B.; Fu, Z.; Jia, Y. Green luminescent center in undoped zinc oxide films deposited on silicon substrates. *Appl. Phys. Lett.* **2001**, *79* (7), 943−945.
(32) Bandopadhyay, K.; Mitra, J. Zn interstitials and O vacancies responsible for n-type ZnO: what do the emission spectra reveal? *RSC Adv.* **2015**, *5* (30), 23540−23547.
(33) Hur, T.-B.; Jeen, G. S.; Hwang, Y.-H.; Kim, H.-K. Photo-luminescence of polycrystalline ZnO under different annealing conditions. *J. Appl. Phys.* **2003**, *94* (9), 5787−5790.
(34) Kim, I. H.; Ku, D. Y.; Ko, J. H.; Kim, D.; Lee, K. S.; Jeong, J. h.; Lee, T. S.; Cheong, B.; Baik, Y. J.; Kim, W. M. Improvement of the thermal and chemical stability of Al doped ZnO films. *J. Electroceram.* **2006**, *17* (2−4), 241−245.
(35) Kida, T.; Nishiyama, A.; Hua, Z.; Suematsu, K.; Yuasa, M.; Shimanoe, K. WO3 Nanolamella Gas Sensor: Porosity Control Using SnO_2 Nanoparticles for Enhanced NO2 Sensing. *Langmuir* **2014**, *30* (9), 2571−2579.
(36) Dieguez, A.; Romano-Rodrıguez, A.; Morante, J.R.; Kappler, J.; Barsan, N.; Gopel, W. Nanoparticle engineering for gas sensor optimization: improved sol−gel fabricated nanocrystalline SnO_2 thick film gas sensor for NO2 detection by calcination, catalytic metal introduction and grinding treatments. *Sens. Actuators, B* **1999**, *60* (2-3), 125−137.
(37) Brillson, L. J.; Lu, Y. ZnO Schottky barriers and Ohmic contacts. *J. Appl. Phys.* **2011**, *109* (12), 121301.
(38) Murphy, T. E.; Blaszczak, J. O.; Moazzami, K.; Bowen, W. E.; Phillips, J. D. Properties of electrical contacts on bulk and epitaxial n-type ZnO. *J. Electron. Mater.* **2005**, *34* (4), 389−394.

https://dx.doi.org/10.1021/acsaelm.0c00321
ACS Appl. Electron. Mater. 2020, 2, 2064−2070